Artificial neural networks applied to the measurement of lateral wheel-rail contact force: a comparison with a harmonic cancellation method

Pedro Urda[a,*], Javier F. Aceituno[b], Sergio Muñoz[c], José Luis Escalona[a]

[a] *Department of Mechanical and Manufacturing Engineering, University of Seville, Spain*
[b] *Department of Mechanical and Mining Engineering, University of Jaén, Spain*
[c] *Department of Materials and Transportation Engineering, University of Seville, Spain*

Abstract

This paper presents a method for the experimental measurement of the wheel-rail lateral contact force based on Artificial Neural Networks (ANN). It is intended to demonstrate how an Artificial Intelligence (AI) method proves to be a valid alternative to other approaches based on sophisticated mathematical models when it is applied to the wheel-rail contact force measurement problem. This manuscript addresses the problem from a computational and experimental approach. The artificial intelligence algorithm has been experimentally tested in a real scenario using a 1:10 instrumented scaled railway vehicle equipped with a dynamometric wheelset running on a 5-inch-wide track. The obtained results show that the ANN approach is an easy and computationally efficient choice to measure the applied lateral force on the instrumented wheel, even requiring a lesser number of sensors involved.

Keywords: Artificial neural network, multibody system, contact-force measurement, scaled railway vehicle, dynamometric wheelset, experimental validation.

1. Introduction

Artificial intelligence has been one of the most active research areas in the field of engineering over the past few decades, especially the use of Artificial Neural Networks (ANNs) applied to the solution of complex problems. Artificial neural networks are computational algorithms inspired by the anatomy of the human brain and the way it works. The brain is a complex and fully non-linear, parallel computer, faster than any other machine. The power of an ANN lies in its parallel processing and learning capabilities, being able to find solutions it was not trained to find. Since their appearance in computational science, ANNs have been widely applied to different subjects such as computational vision, systems control or voice recognition [1, 2, 3, 4].

Railways research is one of these fields that has been traditionally based on the use of sophisticated computational models to analyse the vehicle's dynamics response on interaction with the track, with the purpose of solving problems such as the calculation of the wheel-rail contact points, the adhesion coefficient or the estimation of the wheel-rail contact forces. However, it can be observed in the scientific literature how artificial intelligence has had an increasing presence in railways engineering over the last decade. Recent studies demonstrate that different machine learning approaches can be used as an alternative to the classical computational methods showing promising results. In the work of Falomi et al. [5], a comparison between classical semi-analytical methods and neural networks is presented for the determination of the wheel-rail contact points. ANNs prove to be a valid solution since they require less

*Corresponding author: purda@us.es

computational effort and avoid storing large look-up-tables in memory[6] for the solution of the wheel-rail contact problem.

There are several parameters that are decisive for the vehicle's dynamic response such as the wheel-rail contact forces, the angle of attack between wheel and rail and the adhesion coefficient that are difficult to measure online. Gajdar et al. present in [7] a method for the calculation of the friction coefficient μ based on ANN with excellent results. In this work they evaluate the feasibility of using Recurrent Neural Networks (RNN) [4] to address the problem. Recurrent neural networks use information from previous time steps during their training processes. However, the use of a previous estimation of the friction coefficient as input do not seem to improve the network performance. A similar thesis is the one presented by Malvezzi et al. [8], where the ANNs are used to experimentally estimate the friction coefficient on different test runs conducted with artificially degraded adhesion conditions.

Track maintenance is another important issue in railways engineering. Large track irregularities can jeopardize the safety of the rolling stock. In the work of Sadedhi [9], a method based on ANNs using geometry data from automated inspection vehicles as inputs is presented for the assessment of the track quality conditions. In this work, different types of ANNs are used to predict defects on the rails, the sleepers, the ballast or the fastening system. Huai Chou et al. present in [10] a thought-provoking work where damages on the rails are identified using an ANN and input data from a previous track inspection with electromagnetic and ultrasonic systems. Nakhaee et al. present in [11] an interesting and updated survey of the different applications of the machine learning in rail track maintenance. Some other interesting examples of artificial intelligence applications to track maintenance are: The work of Chen et al. [12] where Neural Networks (NNs) are used to detect failures in the catenary fastener system, o the work of Cheng and Zhao [13] that applies NNs to the fault detection in railway switchings, or the work of Yin et al. [14] that address the fault diagnosis problem of vehicle on-board equipment in high speed trains using artificial intelligence

Artificial neural networks can also be applied to rail wear measuring problem. As it is well known, rail wear is directly related to track maintenance cost, ride comfort and prevention of derailment. In the railways industry, rail wear is normally measured using sophisticated computational vision systems or expensive LIDAR laser scanners. As an alternative, in the work of Shebani [15], a Non-linear Autoregressive model with eXogenous input Neural Network (NARXNN) [4] is used to predict the rail wear based on input parameters such as load, yaw angle, speed, wheel-rail profile, first derivative of wheel-rail profile and second derivative of wheel-rail profile. Another example of ANN applied to the detection of rail defects and wear is presented in [16]. The obtained results show that the ANN can be satisfactorily used to predict rail wear.

The railways industry has had always a great interest in the wheel-rail contact forces, since they strongly determine the dynamic behaviour of the vehicle. Every railway manufacturer or operating company wants to know the value of the contact forces in order to have the highest level of safety on their vehicles. However, as mentioned before, the measurement of wheel-rail contact forces is not an easy task. Traditional methods found in the literature use sophisticated multibody models [17] to estimate the wheel-rail contact forces [18, 19] based on the dynamic response of the vehicle. The main drawback

of these methods is the high computational effort required to solve the dynamic equations, especially when dealing with the wheel-rail contact problem. That means that not all of these computational multibody models can be implemented on vehicles' onboard computers where real-time computing is required. Recent studies, like the one presented by Escalona et al. in [20, 21], try to simplify the wheel-rail contact constraint equation showing as a result a notorious improvement in the model's computational efficiency. However, real-time simulation of the online estimation of wheel-rail contact forces has yet to be achieved. In this regard, ANNs, due to their simplicity and faster performance, represent an interesting option for the online measurement of the wheel-rail contact forces. An instance is the work of Falomi et al. [22] where a multibody model of a railway vehicle is combined with an ANN for the prediction of the contact points and applied forces, showing a low computational burden. In the work of Yifan et al. [23], a method for the continuous measurement of wheel-rail contact forces based on Radial Basis Function Networks (RBFN) [4] is presented. In the work of Gualano [24], the so-called recurrent neural networks [4] are used to estimate the derailment coefficient. The use of this kind of NN is an intend to include the dynamics of the vehicle in the network performance.

Artificial neural networks have also been applied to others subjects in railway engineering as shown next. An example is the work presented by Mingyang Yu et al. [25] where an ANN is used to detect possible obstacles on the track that could compromise the safety of the vehicle. The algorithm proposed proves to be faster than other classical computational vision algorithms. A similar work is presented in [26] where an ANN is used to detect object on the track under shunting mode. According to the authors, the algorithm proposed is able to execute in real time. A completely different use of ANNs on railways is the one proposed in [27], where the networks are use as a tool to predict railways delays in large transportation systems. A similar work is the one presented by Gallo et al. in [28]. In this work, data from the turnstiles passenger counting systems of a metro station are used as inputs of an ANN for forecasting the vehicle's onboard passenger flow. Train re-scheduling problems can also be addressed with artificial intelligence as demonstrated in [29] Another approach is presented by Paneiro et al. in [30], where a prediction method based on ANN for the estimation of induced vibrations on urban areas by railroad vehicles is defined. Finally, in the work of Changwei et al. [31], ANNs are used to evaluate the risk on the construction investment using as inputs different economical and political factors. Based on all of the above, it can be observed how machine learning techniques, such as ANNs are becoming more prevalent in the railways industry.

This paper is intended to demonstrate how artificial intelligence can be applied with promising results to the solution of a problem that in the railways industry has been normally addressed by more extended mechanical engineering methods (Multibody modelling, contact theory, etc.). To that end, two different algorithms for the experimental measurement of the wheel-rail lateral contact force are compared in this work. The first algorithm proposed is a classical method based on a harmonic elimination technique that has been previously applied to the measurement of tyre-road contact forces [32] and wheel-rail contact forces [33]. The second algorithm uses a multi-layer artificial neural network for the estimation of the wheel-rail lateral contact force. As main contribution, this work experimentally validates the use of ANNs on a 1:10 scaled vehicle equipped with a dynamometric wheelset when compared to the harmonic

elimitation technique. The results obtained with both approaches are also compared with the numerical results drawn from a railway computational model [34] developed by the Department of Mechanical and Manufacturing Engineering of the University of Seville showing a good accordance. The obtained results show how the ANN has an equivalent performance to the harmonic cancellation method when measuring the applied lateral force on an instrumented wheel. In the present work, as one of its main novelties, it has been proven how the ANN does not require the measurement of the instantaneous angular position of the instrumented wheel as input, whereas in the harmonic cancellation method, this is necessary for its correct performance. The purpose of this manuscript is also to serve as inspiration to other researches to apply modern artificial intelligence and machine learning techniques to similar railways engineering problems.

This paper is organized as follows: Section 2 summarizes the harmonic cancellation method for the wheel-rail contact force measurement. In Section 3, the ANN based method is presented together with some simulation results. Section 4 presents the experimental set-up used to validate the proposed methods. Section 5 shows the experimental validation of both methodologies with the results obtained during the experimental campaign with the scaled vehicle running on a 5-inch-wide scale track. Summary and conclusions are presented in Section 6.

2. Harmonic cancellation method for the wheel-rail contact force measurement

The first method proposed for the measurement of the lateral contact force is based on a harmonic elimination technique. The algorithm presented in this section is an application of an algorithm developed for the measurement of the tyre-road contact forces. A full description of the aforementioned method can be found in [32]. A similar methodology has also been satisfactorily used to measure the wheel-rail contact forces on a full-scaled railway vehicle [35], and it is still used in some Spanish dynamometric wheelsets belonging to *Talgo*®. At this point, it is important to note that the measurement of the normal contact force on the scaled instrumented wheel is out of the scope of this paper. This is due to the fact that the instrumentation set-ut of the instrumented wheel (see Section 4) does not allow the measurement of the normal contact force. The normal contact force can be estimated through the elongation of the primary suspension, together with some simple kinematic constraints. As mentioned before, all the equations presented below are the result of the application of the general method on a scaled dynamometric wheelset instrumented with a set of strain gauges. A more extended description of this particular method can be found in [36].

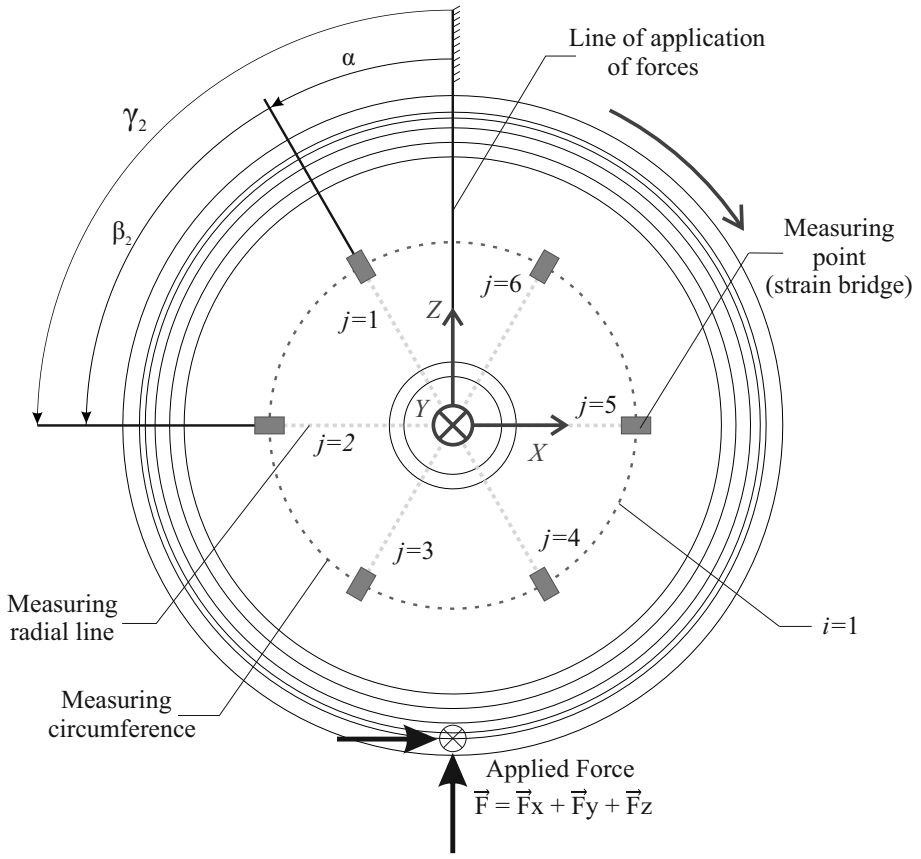


Figure 1: Strain gauges positioning on the instrumented wheel

The harmonic cancellation method used for the measurement of wheel-rail contact forces requires that there is an instrumented railway wheel equipped with strain gauges. Those sensors must be placed at equally spaced angular positions in one or more measuring circumferences. The more sensors, the more harmonics can be cancelled and better precision on the measurement reached. The harmonic cancellation technique removes the effect of the rotation on the strain sensors measurements. Due to the reduced wheel radius of the wheelset used in this work (See Section 4), a unique set of six strain gauges placed on the same measuring circumference has been used. Figure 1 shows a sketch of the instrumented wheel with the strain gauges. In the figure, each one of the six purple rectangles represents a strain bridge. These bridges can be configured as quarter, half or full bridge depending on the particular application. In this case, it has been chosen a half-bridge configuration. That means each strain bridge installed on the wheel includes two strain gauges, one on each side of the wheel-web, located at identical angular position. In such a way, the strain measured by the bridge is the difference between the measured strains by each strain gauge of the bridge. Hereinafter, subscript i refers to the single measuring circumference and subscript j refers to each of the measuring radii. Angle α is the angle between the line of application of the forces and the first measuring radius (reference measuring radius), β_j is the angle between the reference measuring radius and a different measuring radius, and angle γ_j is the angle between an arbitrary measuring radius and the line of application of the forces. Angle γ_j can be determined installing a position encoder on the instrumented wheelset.

Assuming that there is a combination of longitudinal, lateral and vertical forces applied on the wheel

tread resulting on a force $\vec{\mathbf{F}}$, and the wheel is rotating around the Y axis (see Fig. 1), each strain gauge is going to observe $\vec{\mathbf{F}}$ as a force that moves around the wheel. As a result, the radial strain measured on each strain sensor is a function of the applied longitudinal load $F_X(t)$, lateral load $F_Y(t)$ and vertical load $F_Z(t)$, and it can be expressed as follows:

$$\varepsilon_j(\gamma_j, t) = B_j^X(\gamma_j)F_X(t) + A_j^Y(\gamma_j)F_Y(t) + A_j^Z(\gamma_j)F_Z(t) \tag{1}$$

$$\gamma_j = \alpha + \beta_j \tag{2}$$

where B_j^X, A_j^Y and A_j^Z are influence functions that depend on the deformed shape of the wheel-web.

The continuous rotation of the instrumented wheelset while functioning elicits a harmonic behaviour form to the measured radial strain. Thus, it can be written as a Fourier series expansion of infinite terms:

$$\varepsilon_j(\gamma_j, t) = F_X(t)\sum_{k=0}^{\infty} B_k^X sin(k\gamma_j) + F_Y(t)\sum_{k=0}^{\infty} A_k^Y cos(k\gamma_j) + F_Z(t)\sum_{k=0}^{\infty} A_k^Z cos(k\gamma_j) \tag{3}$$

Equation 3 assumes that the lateral component F_Y and the vertical component F_Z of the applied force on the instrumented wheel yield symmetric strains with respect to a diametrical and vertical plane on the wheel. On the other hand, the longitudinal component F_X of the applied force results on anti symmetrical strains on the wheel.

Considering that, a high precision of the measurement can be reached using just the first n harmonic, Eq. 3 can be written in matrix form as:

$$\begin{aligned}\varepsilon_j(\gamma_j, t) = &\begin{bmatrix}1 & cos(\gamma_j) & cos(2\gamma_j) & \cdots & cos(n\gamma_j)\end{bmatrix}\begin{bmatrix}A_0^Y & A_0^Z\\ A_1^Y & A_1^Z\\ \vdots & \vdots\\ A_n^Y & A_n^Z\end{bmatrix}\begin{bmatrix}F_Y(t)\\ F_Z(t)\end{bmatrix} + \\ &\begin{bmatrix}0 & sin(\gamma_j) & sin(2\gamma_j) & \cdots & sin(n\gamma_j)\end{bmatrix}\begin{bmatrix}B_0^X\\ B_1^X\\ \vdots\\ B_n^X\end{bmatrix}\begin{bmatrix}F_X(t)\end{bmatrix}\end{aligned} \tag{4}$$

The terms of the coefficient matrix can be easily obtained though the Fourier series expansion, known the normalized deformed shape of the wheel when isolated longitudinal, lateral and vertical load are applied on it. These normalized deformed shapes have been determined using a Finite Element Model (FEM) of the wheel developed in ANSYS®. Then, using the optimization procedure explained in [32], the following system of equations is obtained:

$$\begin{bmatrix}A_1^Y & A_1^Z\\ A_2^Y & A_2^Z\end{bmatrix}\begin{bmatrix}F_Y(t)\\ F_Z(t)\end{bmatrix} = \begin{bmatrix}E_S\\ E_A\end{bmatrix} \tag{5}$$

$$\begin{bmatrix}B_1^X\\ B_2^X\end{bmatrix}\begin{bmatrix}F_X(t)\end{bmatrix} = \begin{bmatrix}E'_S\\ E'_A\end{bmatrix} \tag{6}$$

where,

$$E_S = \frac{1}{3}\sum_{j=1}^{6}(\varepsilon_j cos(\gamma_j)) \tag{7}$$

$$E_A = \frac{1}{3}\sum_{j=1}^{6}(\varepsilon_j sin(\gamma_j)) \tag{8}$$

$$E'_S = \frac{1}{3}\sum_{j=1}^{6}(\varepsilon_j cos(2\gamma_j)) \tag{9}$$

$$E'_A = \frac{1}{3}\sum_{j=1}^{6}(\varepsilon_j sin(2\gamma_j)) \tag{10}$$

and,

$$\gamma_j = \alpha + (j-1)\frac{\pi}{3} \tag{11}$$

Finally, when the instantaneous measurement of the six strain bridges and the angular position of the wheel are known, the applied lateral force on the wheel $F_Y(t)$ can be drawn from Eq. 5.

3. Lateral contact force measurement with ANNs

An ANN is a mathematical algorithm that attempts to reproduce the way the human brain solves arbitrary problems. In the same way that humans use their previous experiences to solve new problems or challenging situations, an ANN takes solved problems as examples to build an intelligent system that is capable of making decisions or carrying out classification tasks. Since their first appearance around 1943, ANNs have been constantly evolving. Nowadays, the most modern formulation of an ANN is the so-called Spiking Neural Network (SNN), that includes differential equations on its formulation. As explained in the work of Perez et al. [37], SNNs have the advantage of being dependent on time which makes them suitable for advanced control of systems. However, they are not as easily applicable to the solution of general problems as are convectional ANNs.

A neural network consists of cells (also call neurons) and links. The cells are the computational part of the network being in charge of the reasoning and generation of the activation signals. Links connect the different neurons and transmit the information along the network. Links are affected by the so-called weight w_i and biases b_j of the net. The perceptron (see Fig. 2 (a)) represents the simplest form of an ANN. This simple structure receives as input a linear combination of the networks's inputs. The inner function of the neuron can be linear or non-linear and include biases or not. The perceptron model is appropriate for the solution of simple problems. However, for the solution of more complex problems, multilayer network architectures are required. As depicted in Fig. 2 (b), a multilayer ANN can include a larger number of neurons distributed across several hidden layers. Both the perceptron and the multilayer ANN can have one or more outputs depending on the problem they are applied to.

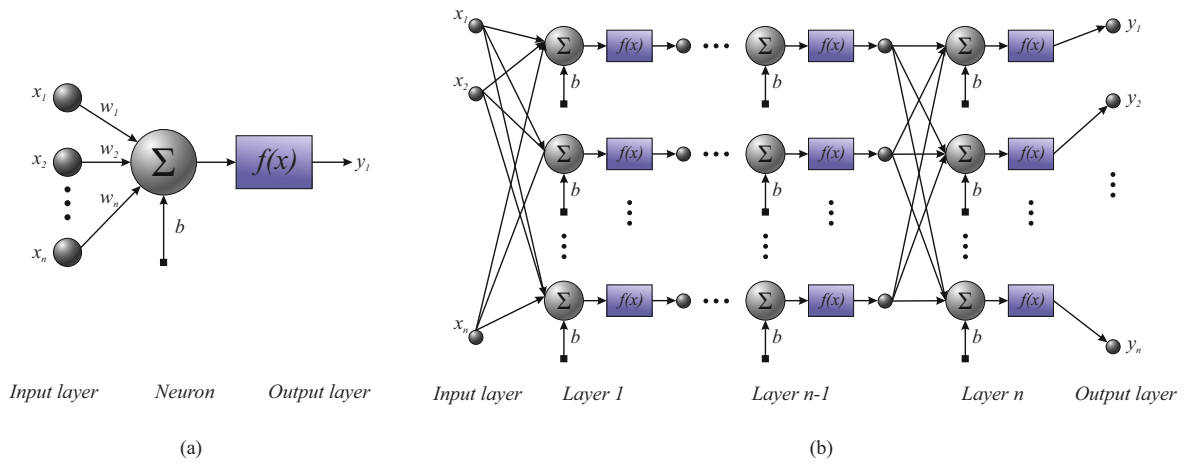


Figure 2: (a) Perceptron model. (b) Multilayer ANN

3.1. ANN definition and training

In this work, a multilayer ANN with multiple inputs and a single output has been used for the lateral contact force estimation. The network definition and training process have been accomplished using the *MATLAB*® Neural Network Toolbox functions [38]. Different network architectures and training algorithms have been tested in order to find the optimal network. The ultimate goal is to find an ANN able to estimate the lateral contact force applied on the instrumented wheel with equivalent performance to the classical harmonic cancellation technique presented in Section 2. In this regard, just like the harmonic cancellation method, the proposed ANN must calculate the applied lateral force using the radial strain measured by the strain bridges and the instantaneous angular position of the wheelset as inputs.

As previously mentioned, the ANN must be trained using an input data set whose output results were known in advance (supervised training). In this case, the training data have been obtained using the FEM of the instrumented wheel (see Fig. 3 (a)). The model has been experimentally validated during the dynamometric wheelset calibration process [36] making sure it fully represents the mechanical behaviour of the real wheel. During its calibration the instrumented wheel was loaded with different combinations of vertical loads in order to stablish a relationship between applied loads and measured strains. Assuming that the normalized deformed shapes of the instrumented wheel when unitary vertical and lateral loads are applied on it (see Fig. 3 (b) and (c) respectively, are obtained during the calibration process), a synthesized training data set, like the one shown in Fig. 4, can be obtained. The radial strains depicted in the figure have been obtained assuming that the instrumented wheelset moves at constant angular velocity along the track while a combination of lateral and vertical loads, depicted in Fig. 5 (a) and (b) respectively, is applied on it. As a result, it can be observed in the figure, a set of six graph lines of different colour that represent the radial strain measured by each of the strain bridges installed on the wheel-web (see Fig. 1). In Fig. 4 it can be observed how the magnitudes of the measured radial strains on the wheel-web by the six strain bridges varies due to the effect of the applied loads. It must be noted that the influence of the longitudinal load is not considered when synthesising training data.

In this particular case, considering the actual instrumentation, it has been proved that the effect of the longitudinal load in the measured radial strain can be neglected.

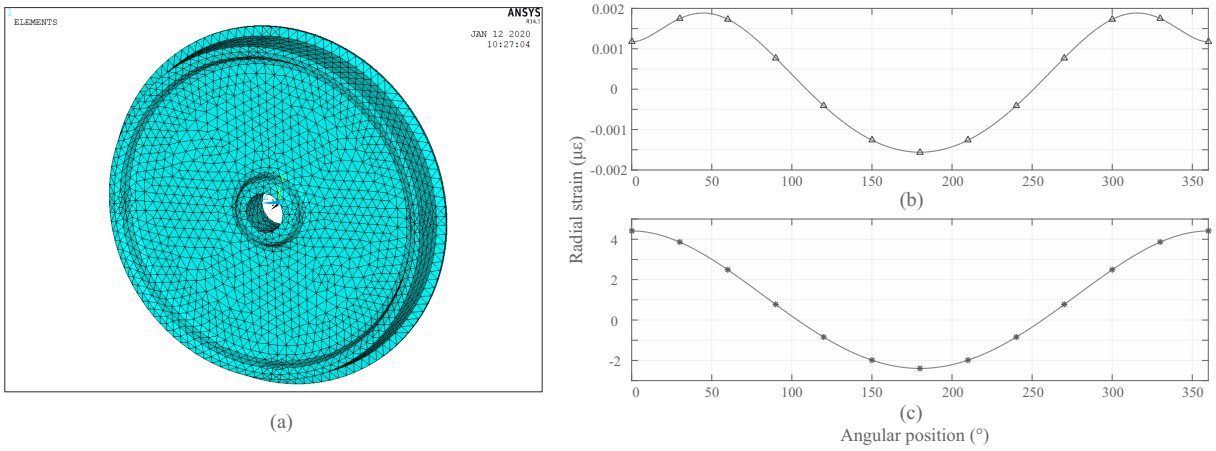


Figure 3: (a) Instrumented wheel FEM. (b) Normalized deformed shape under vertical load influence. (c) Normalized deformed shape under lateral load influence

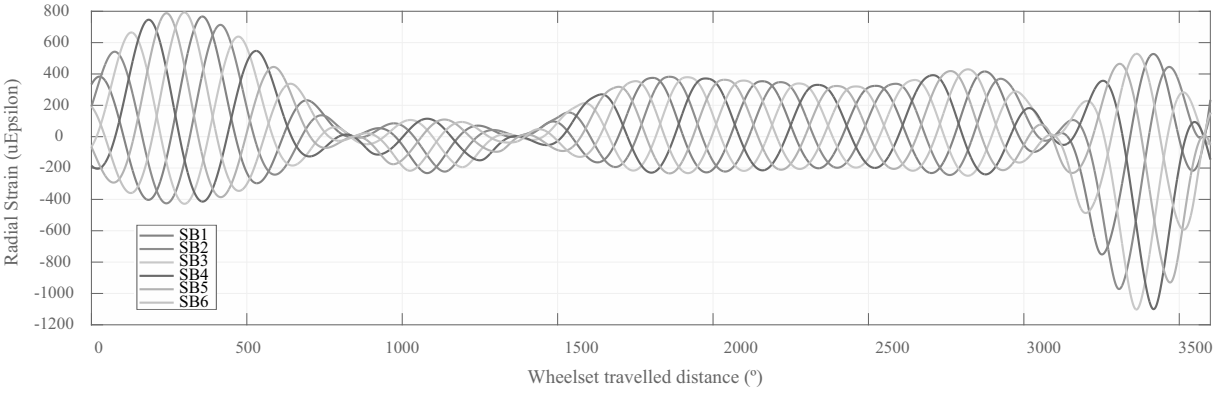


Figure 4: Synthesized radial strains for network training

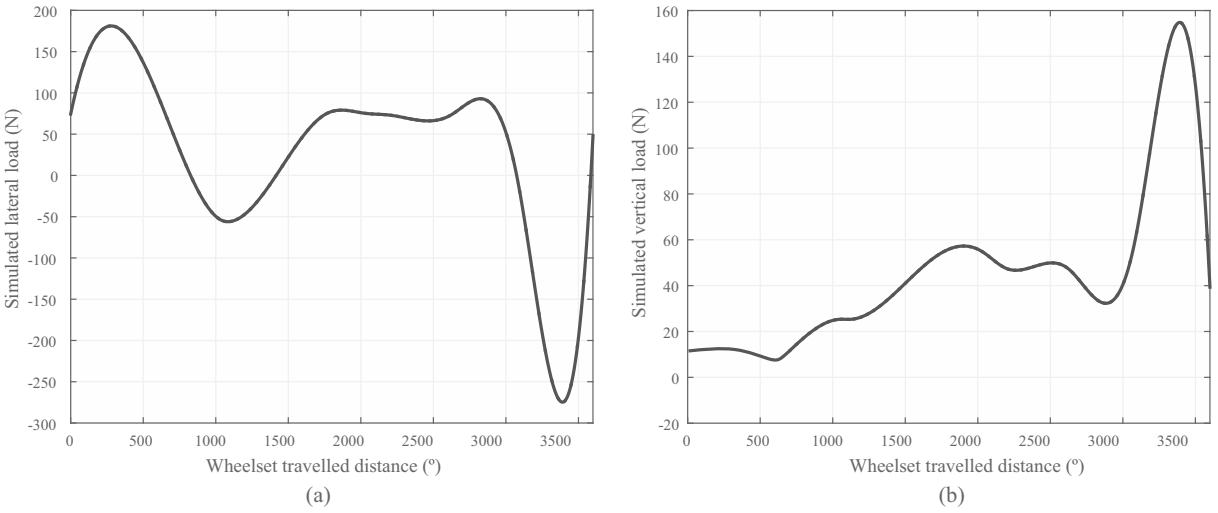


Figure 5: (a) Assumed lateral load. (b) Assumed vertical load

The training process of the ANN is not a trivial task. In fact, the success of the training and the correct final performance of the network partly depends on the programmer experience. The Back-Propagation (BP) algorithm is the method most commonly used for training the network. The algorithm changes the weights and biases of the net based on the Mean Squared Error (MSE) of the network's outputs with respect to the reference solution. This is called supervised training. In this work, different BP network architectures and training functions have been tested in order to find the fastest and most precise network to estimate the lateral contact force applied on the instrumented wheel. To that end, an arbitrary training data set similar to the one shown in Fig. 4 and Fig. 5, but considering variable forward velocities of the wheelset and a larger number of data, has been used for training the network. In order to have an optimal performance during the training process and avoid possible over-fitting problems [4], the data are divided for training in three sets: 80% for training, 15% for validation and 5% for testing.

Table 1 summarizes the number of training epochs, training time and MSE of the network using different training functions when a $\{10-5\}$ ANN is used. This network has two hidden layers with 10 and 5 neurons on each. Hereinafter, this is the way ANN architectures are going to be defined in this paper. As it can be observed, after an identical number of training epochs, the network N1 that uses the *Levenberg-Marquardt* training function shows the best performance. However, it is also the slowest to train. This efficiency analysis has been accomplished using an Intel® Core™ i7-3770 3.40 GHz and 32 GB RAM.

The influence of network architecture on its performance has been also analysed. Table 2 shows a comparison between four ANN with different numbers of hidden layers and neurons. It is easily observed how an increase in the number of neurons or the number of neurons and layers maintaining the same number of training epochs results in a better performance (smaller MSE). The drawback of using a more complex network architecture is not only the greater time consumption during the training process but also the risk of overfitting when dealing with almost linear problems. The increase of the number of training epochs on the $\{10-5\}$ network also improves the network performance slightly, although not

as much as the increase of neurons or layers. It is also observed in Table 2 that the network N1b with a single hidden layer has an equivalent performance to network N1 which has two hidden layers. This is something expected since, as explained by Hornik et al. in [39], it can be proved that a feedforward neural network with one hidden layer can approximate any continuous function with sufficient accuracy provided that the single hidden layer has enough number of neural units.

Table 1: Network training functions efficiency analysis

Network	**Training function**	**Epochs**	**Training time (s)**	**MSE (N)**
N1 $\{10-5\}$	Levenberg-Marquardt	2000	383	$3.0 \cdot 10^{-4}$
N2 $\{10-5\}$	Polak-Ribiére Conjugate Gradient	2000	89	$6.6 \cdot 10^{-3}$
N3 $\{10-5\}$	Fletcher-Powell Conjugate Gradient	2000	89	$1.7 \cdot 10^{-3}$
N4 $\{10-5\}$	One Step Secant	2000	79	$5.8 \cdot 10^{-3}$
N5 $\{10-5\}$	Resilient Backpropagation	2000	15	$5.5 \cdot 10^{-2}$
N6 $\{10-5\}$	Scaled Conjugate Gradient	2000	28	$7.5 \cdot 10^{-3}$
N7 $\{10-5\}$	BFGS Quasi-Newton	2000	88	1.5
N8 $\{10-5\}$	Variable Learning Rate	2000	15	1.9
N9 $\{10-5\}$	Conjugate Gradient	2000	28	$3.5 \cdot 10^{-3}$

Table 2: Network architecture performance analysis

Network	**Training function**	**Epochs**	**Training time (s)**	**MSE (N)**
N1 $\{10-5\}$	Levenberg-Marquardt	2000	383	$3.0 \cdot 10^{-4}$
N1a $\{20-10-5\}$	Levenberg-Marquardt	2000	713	$7.3 \cdot 10^{-5}$
N1b $\{20\}$	Levenberg-Marquardt	2000	383	$3.0 \cdot 10^{-4}$
N1c $\{10\}$	Levenberg-Marquardt	2000	331	$7.8 \cdot 10^{-4}$
N1c $\{10-5\}$	Levenberg-Marquardt	5000	978	$1.3 \cdot 10^{-4}$

In an attempt to demonstrate the potential of the ANN for the lateral contact force estimation, a $\{10-5\}$ network that uses only the measurements of the six strain bridges installed on the instrumented wheel as inputs and removing the angular position measurement has also been programmed and tested. As a result, it has been observed that this simpler network is able to satisfactorily estimate the lateral contact force applied on the wheel, even without knowing the instantaneous angular position of the wheelset measured by the front encoder (see Section 4). This event represents a clear advantage of the ANN approach with respect to the harmonic cancellation method due to the fact that the latter mandatory requires the encoder measurement for its correct performance. Figure 6 shows a comparison between the lateral force estimated with the original seven input network and the reduced version with only six inputs (the one without the encoder measurement). As it is observed, both graph lines almost coincide.

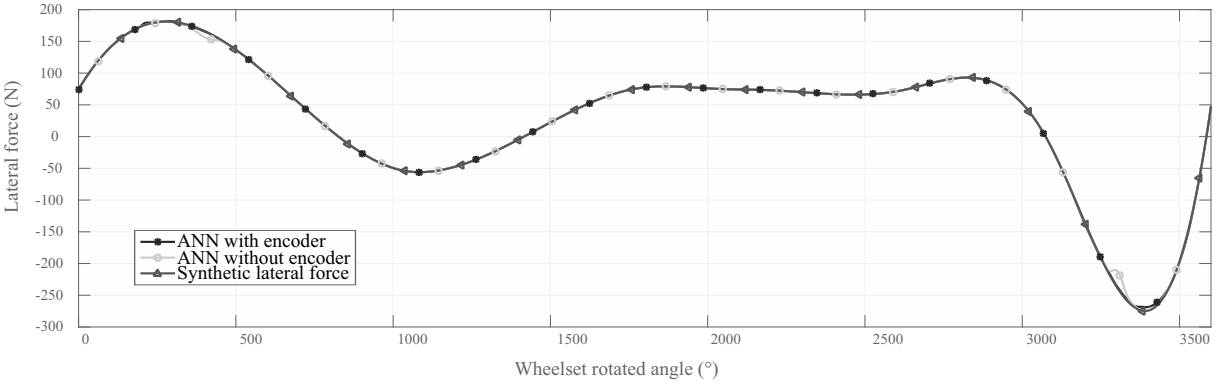


Figure 6: ANN with and without encoder performance comparison

Finally, the performance of the ANN proposed before has been compared with a Recurrent Neural Network (RNN). This kind of NN has feedback connections, that makes the network able to learn the temporal characteristics of the data set. In this particular case the new proposed RNN also includes (in addition to the the measured radial strain) force estimations of previous time steps as inputs. This RNN has been also trained considering and not considering the angular position of the wheelset measured by the encoder. The RNN has a $\{10-5\}$ architecture. The obtained results are shown in Fig. 7. It is observed that the RNN has an excellent accordance with the synthesized lateral force as the regular ANN proposed before. Due to the fact that this kind of NN has a more sophisticated implementation and the obtained results do not prove a notorious improvement with respect to the regular NN, this architecture has not been finally adopted in this work.

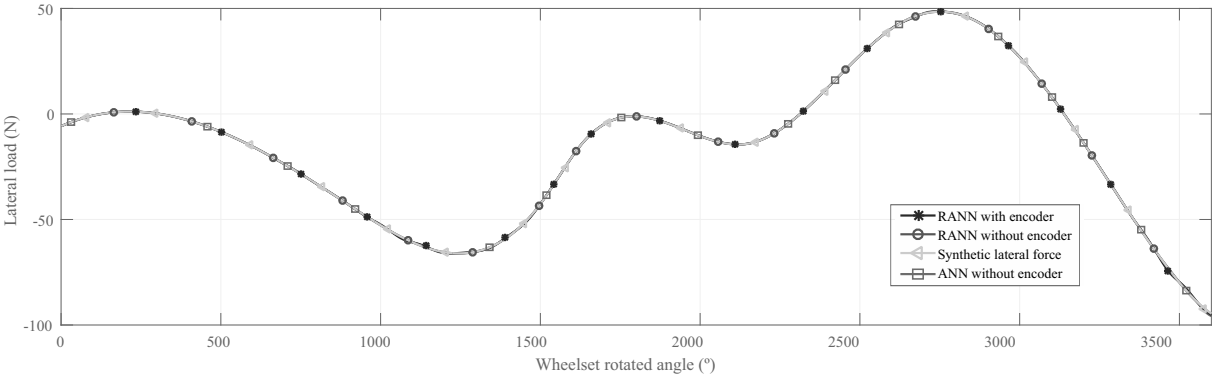


Figure 7: Comparison between recurrent and no recurrent neural networks

3.2. ANN approach comparison with the harmonic cancellation method

In view of the results obtained in the previous subsection, it can be concluded that an ANN with $\{10-5\}$ structure trained with the *Levenberg-Marquardt* algorithm after 2000 epochs shows an excellent performance. The proposed ANN estimates the lateral contact force using only the radial strain on the wheel-web measured by the strain sensors, excluding the measurement of the encoder. Before its final test with real experimental data, the ANN performance has been compared with the classical harmonic cancellation method. Figure 8 shows the obtained results. As it can be observed, there is a good

accordance between both sets of data and the reference force value. However, the two magnifications included in the figure demonstrate how the harmonic cancellation method (dark blue graph line) presents slight oscillations around the reference force value (depicted in red). This is due to the fact that the harmonic cancellation method considers a reduced set of harmonic on its formulation as explained in Section 2. However, the ANN method considers the full spectrum. On the other hand, the ANN result (coloured in light green) perfectly fits the reference data. Both the ANN and the classical method use the same input data set depicted in Fig. 9 that assumes a constant forward velocity of the vehicle.

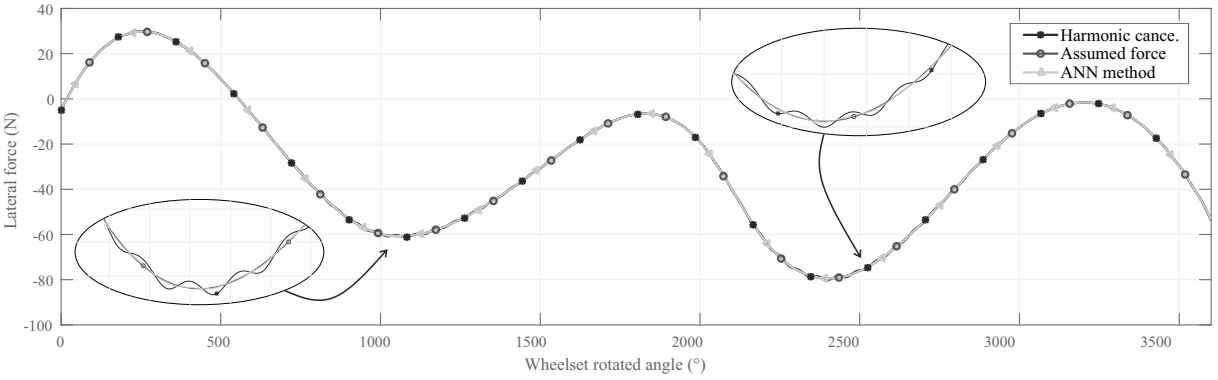


Figure 8: ANN approach vs harmonic cancellation method

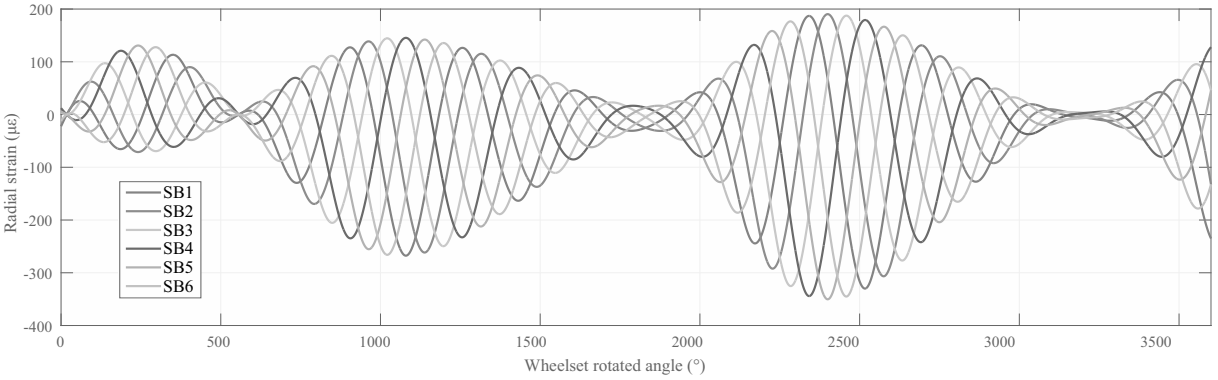


Figure 9: Simulated radial strains instance

The synthesized input data set shown in Fig. 9 is generated assuming a constant forward velocity of the vehicle. However, in real operation conditions the vehicle's forward velocity changes over time. In a final test the ANN method has been tested using a synthesized input data set that assumes variable forward velocity. Figure 10 shows the velocity profile used to synthesized the input data. The estimated lateral force on the wheel using the ANN compared with the harmonic cancellation method is shown in Fig. 11. As it is observed, the ANN satisfactory estimates the lateral force as well as the harmonic cancellation method. The ANN used in this experiment is the $\{10-5\}$ structure (without including the encoder as input) used before in this epigraph. In light of the obtained results, it can be concluded that the ANN method based for the applied lateral force measurement is also valid even when dealing with a variable forward velocity of the vehicle. Figure 12 depicts the synthesized input data set used in this last

300 experiment.

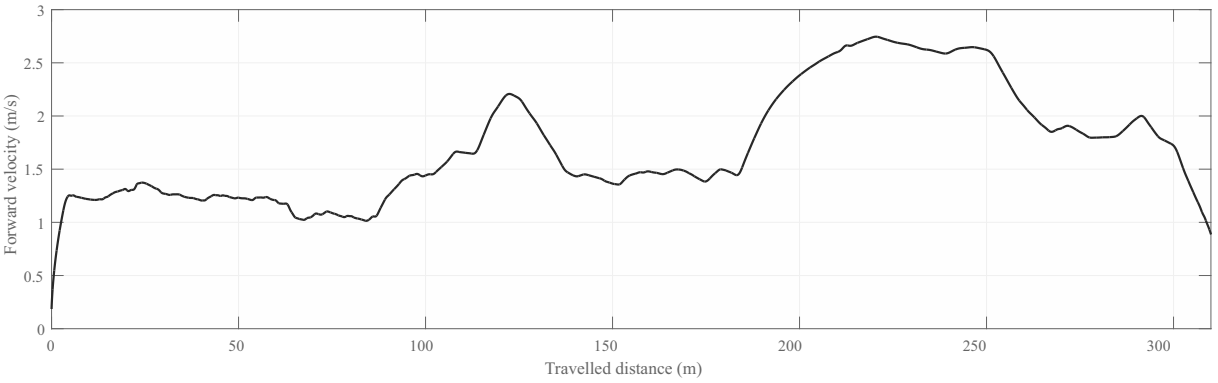


Figure 10: Variable forward velocity profile

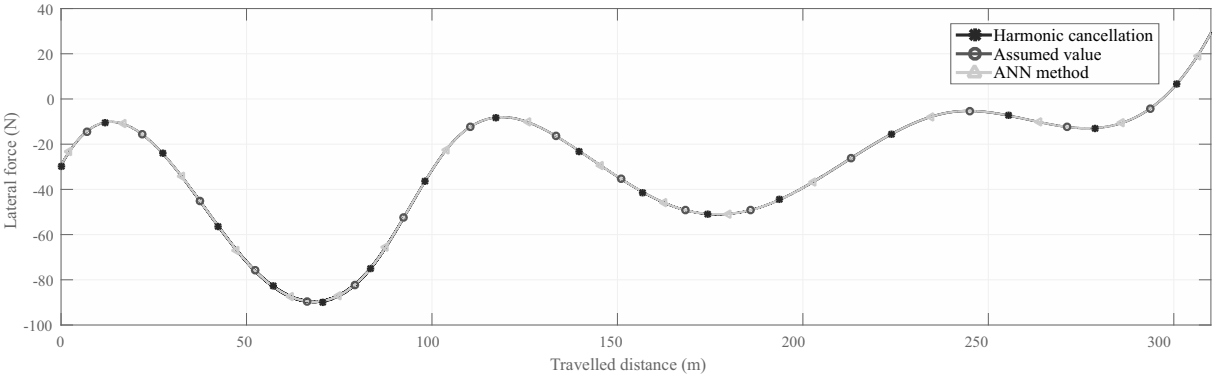


Figure 11: Estimated lateral force assuming variable forward velocity

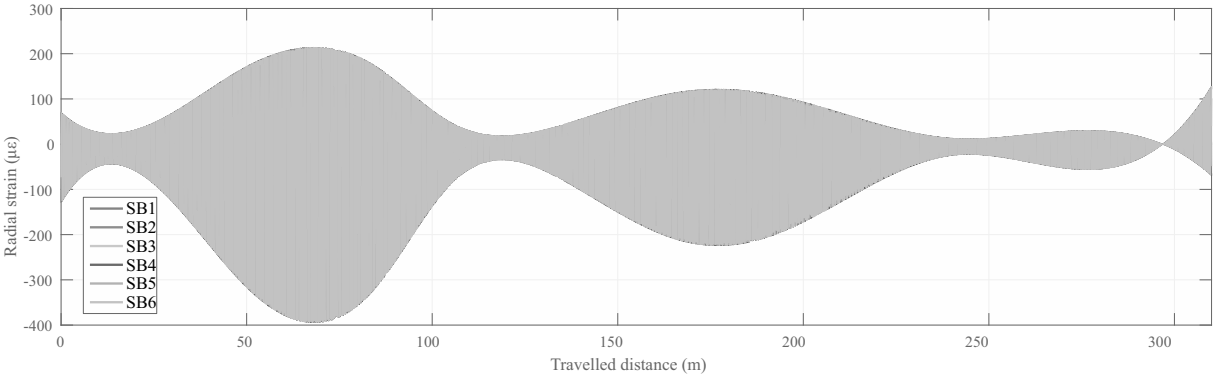


Figure 12: Simulated radial strains assuming variable forward velocity

301 ## 4. Scaled track and instrumented vehicle

302 In the previous section, the ANN method based for the measurement of the lateral contact force, has
303 been tested using synthesized data drawn from the FEM. Its performance has been compared with the

convectional harmonics cancellation approach showing an excellent agreement between both methods. However, this work is intended to go one step further and demonstrate how the ANN also works in a real scenario. To do that, several experiments have been carried out using an instrumented scaled vehicle running on a scaled track.

Figure 13 shows on the left an aerial view of the aforementioned track. It is built on the roof top of the School of Engineering of the University of Seville. It is a 90 meter long and 5 inch wide track. In order to emulate a real track geometry, the horizontal projection of the scaled track includes a set of tangent sections, transitions and constant radius sections. Table 3 summarizes the different sections of the track and their respective lengths. The rails are a miniature reproduction of a standard UIC-54 rail profile machined using stainless steel. They are supported by a set of mechanisms that simulate the track sleepers. Figure 13 (b) shows the rails and the mechanisms. As it is observed, a set of metallic benches hold the track. It is important to note that the mechanisms are not just a simple support for the rails, but they also allow the generation of artificial track irregularities. To do that, every single mechanism allows the variation of the track gauge, the cant angle and the relative height between rails. Prior to accomplishing the experiments, the real track geometry and its irregularities were measured using a high precision total station.



(a) (b)

Figure 13: (a) Experimental scaled track aerial view. (b) Experimental scaled track construction

Table 3: Experimental scaled track ideal geometry

Section	Length	Section type
A	22 m	Tangent
B	3 m	Transition
C	26 m	Constant radius
D	3 m	Transition
E	6 m	Tangent
F	3 m	Transition
G	12 m	Constant radius
H	3 m	Transition
I	12 m	Tangent

Together with the scaled track, the second element necessary to carry out the experiments is the instrumented 1 : 10 scaled vehicle that is shown in Fig. 14 (a). As it can be observed, it is a single bogie that includes two wheelsets and a bogie frame connected by a primary suspension with eight helical springs. All the parameters of the vehicle (dimensions, body mass and spring stiffness) have been experimentally measured at the laboratory. Inertias were determined through the Computer-Aided Design (CAD) of the vehicle developed with Solidworks®. This scaled vehicle is an updated version of another one previously designed and built by the Department of Mechanical Engineering of the University of Seville. The scaling strategy followed during the designing process can be found in [40]. Although the use of a scaled mock-up of a real railroad vehicle is never going to be fully representative of the real mechanical system, a scaled model represents an easy, relatively inexpensive and safe way to analyse its dynamics performance without compromising the safety of passengers or the track integrity.

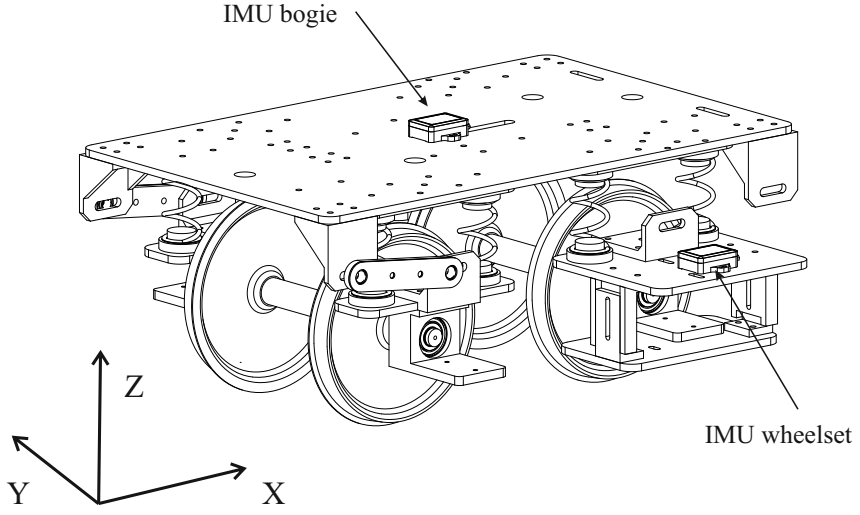
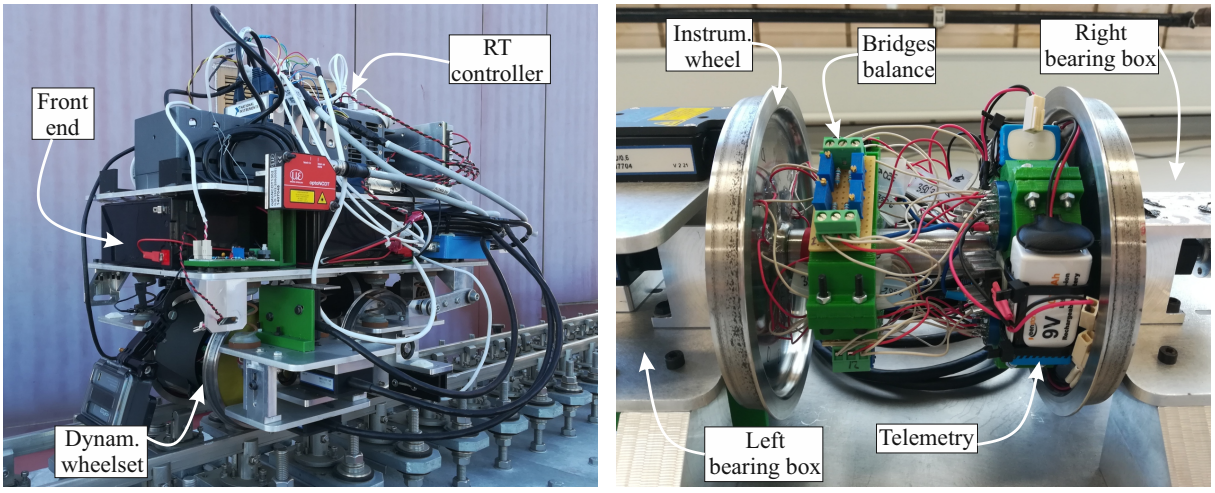


Figure 14: CAD of the experimental scaled vehicle

Figure 15 (a), shows the instrumented vehicle on the scaled track, where it can be observed the different sensors and electronics the vehicles is equipped with. Among them, it is highlighted the presence of two

Inertial Measurement Units (IMU). One is installed on the front wheelset left bearing box, and the second one is placed at the geometric centre of the bogie frame. These two sensors register the acceleration and angular velocities of the bodies where they are installed on. Two precision encoders are mounted on the front and rear wheelset respectively. They are used to calculate the instantaneous position and velocity of the bogie on the track. A 24W DC motor powers the vehicle. A Real Time (RT) computer NI-cRIO-9035 controls the entire system and acquires the sensors' raw measurements at a sampling rate of 500 Hz by means of an 14 bits ADC. Acquired data are processed and filtered in a posterior stage. The master piece of the scaled bogie's instrumentation is its dynamometric wheelset (see Fig. 15 (b)). This wheelset has its left wheel instrumented with a set of twelve strain gauges, six on each side of the wheel. Figure 16 shows the CAD front left and right view of the instrumented wheelset. In the figure the strain gauges installed on the wheel-web have been coloured in purple. It must be point out that the strain gauges are positioned in both sides of the wheel at identical radial and angular positions. Taking into account that the strain gauges rotate with the wheelset, a telemetry system is required to transmit the sensors' measurement to the Data AcQuisition (DAQ) system. The telemetry system is powered by three 9 volts batteries docked to the axle together with three radio transmitters. The transmitter are in charge of the signal conditioning and amplification before sending it to the DAQ system. The strain gauges are connected in pairs (one from each side of the wheel) in half-bridge configuration [41]. This electrical connection of the strain bridges has the advantage of being highly sensitive to the bending experienced by the wheel-web due to the lateral contact force applied on it. To balance the other half of the bridge a set of resistor and high precision potentiometer are also docked to the axel as depicted in Fig. 15 (b). It must be noted that the electrical configuration of the strain bridges does not allow the vertical contact force measurement. To solve that, there are two distance lasers installed at both sides of the bogie registering the instantaneous deflection experienced by the primary suspension. Using this measurement and a simple kinematics model, the applied vertical force on the instrumented wheel can be determined. The dynamometric wheelset was previously precisely calibrated on a static calibration bench. According to this calibration process the force measurements have a maximum uncertainty of ± 2.5 N. A more extended description of the dynamometric wheelset design, instrumentation and calibration process can be found in [36]. A video camera is also installed in the vehicle. It is focused to the instrumented wheel and rail contact point. The acquired images are used to better understand the dynamics phenomena registered by the inertial and force sensors. Table 4 summarizes the instrumentation the vehicle is equipped with.



(a) (b)

Figure 15: (a) Instrumented bogie on the track. (b) Dynamometric wheelset

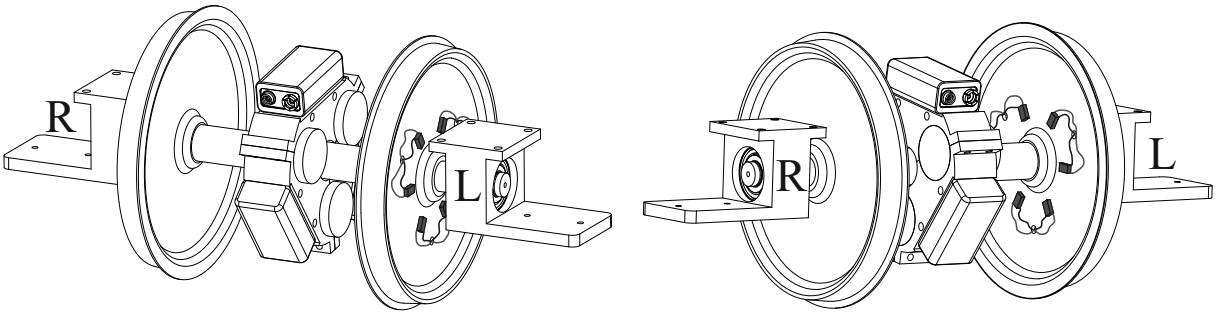


Figure 16: (a) Front left view of the dynamometric wheelset. (b) Front right view of the dynamometric wheelset

Table 4: Instrumentation of the vehicle

Element	**Function**
NI-cRIO-9035	Vehicle control and data acquisition
IMU 1	Front wheelset inertial measurements
IMU 2	Bogie frame inertial measurement
Position encoder 1	Front wheelset angular position measurement
Position encoder 2	Rear wheelset angular position measurement
Distance lasers 1 and 2	Primary suspension deflection measurement
Strain gauges and telemetry	Lateral force measurement
Phidget 24W DC motor	Traction of the vehicle
Batteries 12V	Energization of the vehicle
Video camera	Wheel-rail contact analysis

5. Experimental results and comparison

As explained before, the main goal of this work is to demonstrate the real capabilities of an ANN for the lateral contact force estimation on a railway vehicle. To that end, a set of six experiments have been conducted on the scaled track facilities of the University of Seville using the scaled vehicle presented in the previous section. In these experiments, the vehicle moved on both directions of the track. This is an important point because, as explained in Section 4, the dynamometric wheelset has just one of its two wheels instrumented. That means the forces measured by the instrumented wheel are going to show a different pattern depending on the travelled direction. The radial strains measured on the experiments were used as inputs for the ANN and the classical harmonic cancellation algorithm whose performance is compared. At the same time, the obtained results are also faced with the force estimated using a computational multibody model of the scaled vehicle. It must be noted that, vehicle's bodies and track flexibility are not considered in the simulation model. That can lead to slight imprecision during the experimental validation process. This railways model has been fully developed by the Department of Mechanical Engineering at the University of Seville [34]. The experimental campaign has been carried out under controlled laboratory conditions in order to guarantee the maximum rigour and precision in the measured results.

5.1. Experiments in the forward direction

Three of the six experiments have been conducted with the vehicle moving at 1.5, 2.0 and 2.5 m/s in the forward direction of the track (from point A to point B on Fig. 13 (a)). In these three cases the instrumented wheel (the one left of the dynamometric wheelset) is going to interact with the outer rail in the large radius curve of the track and with the inner rail in the sharp radius curve (the last one of the track in this direction). Figure 17 shows the measured lateral force drawn from the two force estimation algorithms and the multibody simulation model when the vehicle moves at 2.5 m/s. As it can be seen, there is a good accordance between the lateral force estimated by the ANN and the classical harmonic cancellation method. It is also observed how both measuring methods present a good frequency agreement. The multibody model also shows a similar pattern to both experimental approaches. This is a very interesting point since the experimental methods and the simulation model have been developed separately and they do not use the same inputs. The simulation model makes its estimation known the vehicle's parameters, the velocity profile during the experiment and the track geometry. In spite of that, simulations and experiments converge to similar results. Moreover, in this experiment, it is observed how between travelled distance $s = 22$ m and $s = 54$ m, which corresponds with the large radius curve, the instrumented wheel experienced instantaneous flange impacts with the outer rail that induce large fluctuations on the measured lateral force. Note that, these force peaks are captured by the ANN, the harmonic cancellation method and the simulation model at the same time. This intermittent flange contact can be also observed in Fig. 19 that shows two video frames recorded when the vehicle is negotiating the large radius curve. In the frame shown on the left, the vehicle is approximately at position $s = 35$ m. It can be observed how the flange and the rail are in contact. In the frame shown on the right the vehicles is approximately located at $s = 36$ m. In this case a small gap between the

wheel and the rail is observed. In the recorded video it can be seen how the instrumented wheel moves right and left in the image verifying these flange impacts detected by the sensors and estimated by the numerical model. After that, when the vehicle negotiates the sharp radius curve, located between $s = 60$ m and $s = 78$ m, the estimated lateral force shows a more stable value. This is due to the fact that in this second curve, the dynamometric wheelset experienced a quasi-permanent flange contact on the non-instrumented wheel. This is another interesting result concerning the comparison with the computational model adopted in this work. While the computational model accounts for an elastic-penetration hertzian based flange contact approach between the wheel-flange and rail surfaces, the parameters that account for such flange contact (stiffness and damping hertzian parameters) are not constant and depend on the wheel-rail interface. As a result, the adopted parameters reproduced a permanent flange contact in the sharp radius curve, that actually is a quasi-permanent permanent flange contact, as shown by both experimental methods.

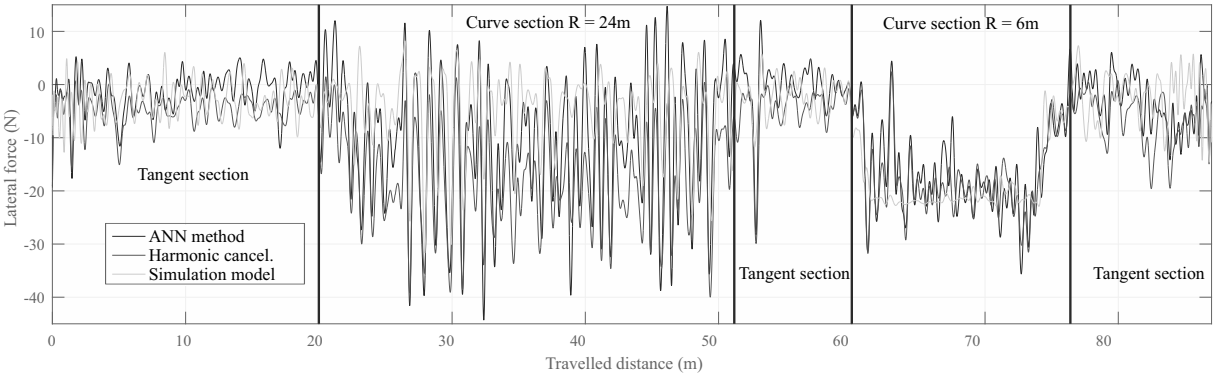


Figure 17: Applied lateral force on the instrumented wheel. Methods comparison in experiment 3

The velocity profile during the experiment is depicted in Fig. 18. It is observed how at the beginning of the experiment, the velocity profile shows some fluctuations around the velocity setpoint. This is due to the action of the PI controller.

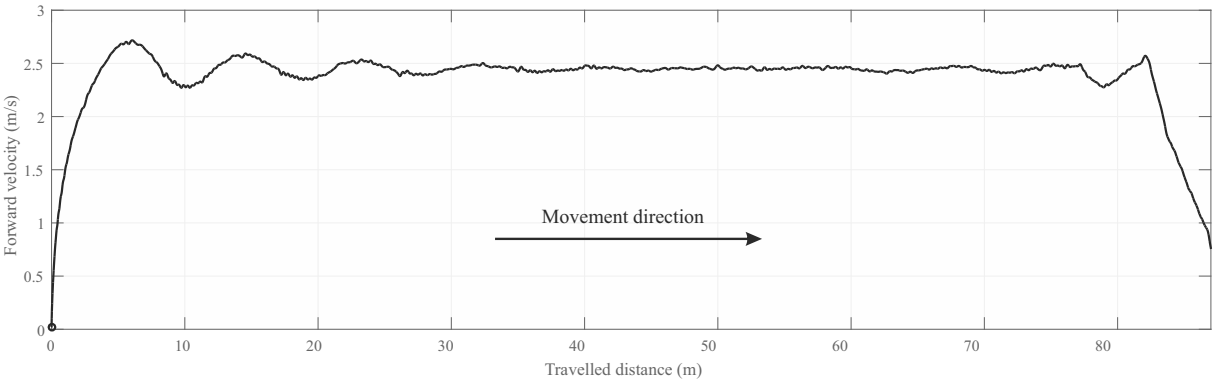
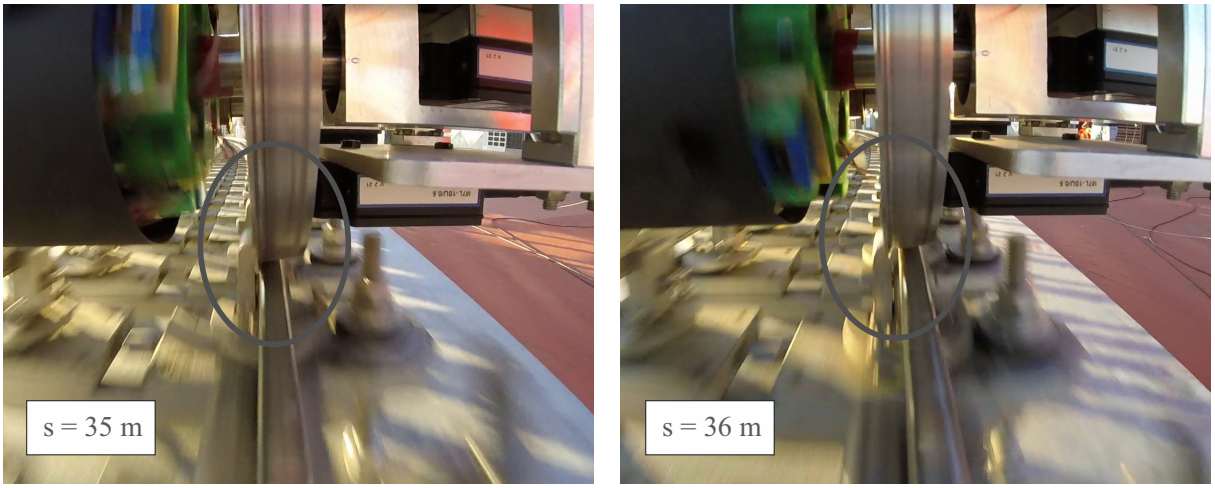


Figure 18: Vehicle's forward velocity



(a) (b)

Figure 19: Instrumented wheel and rail interaction in the large radius curve at two different positions along the track

5.2. Experiments in the backward direction

Similar conclusions can be drawn from the experiments done with the vehicle moving in the backward direction of the track (from point B to point A on Fig. 13 (a)). As an example, Fig. 20 shows another comparison between the applied lateral force estimated with the ANN and the classical method. In this experiment, the vehicle was moving at 1.5 m/s as it can be seen in Fig. 21. In this new scenario, it is also observed how the ANN produces equivalent results to the harmonic elimination approach in terms of amplitude and frequency contents. It is important to note that in this experiment, the magnitude of the measured lateral force on the sharp radius curve (located between $s = 60$ m and $s = 78$ m) is larger than in the previous experiment when the vehicle was moving in the forward direction. This is because in the experiments where the vehicle is moving backwards, the instrumented wheel is the one that experiences the quasi-permanent flange contact. In here, it is also shown that the adopted parameters for the flange contact in the computational model, do not reproduce de quasi-permanent contact as the experimental method do. Figure 22 shows a couple of pictures of the instrumented wheel taken when the vehicle was negotiating the sharp radius curve. It can be observed how there is no gap between the wheel and the rail in any of them. In the full video it is observed how the quasi-permanent contact remains constant along all the small radius curve. Note that in the backward movement coordinates s decreases. That means in Figs. 20 and 21 the experiments begins at $s = 87$ meters.

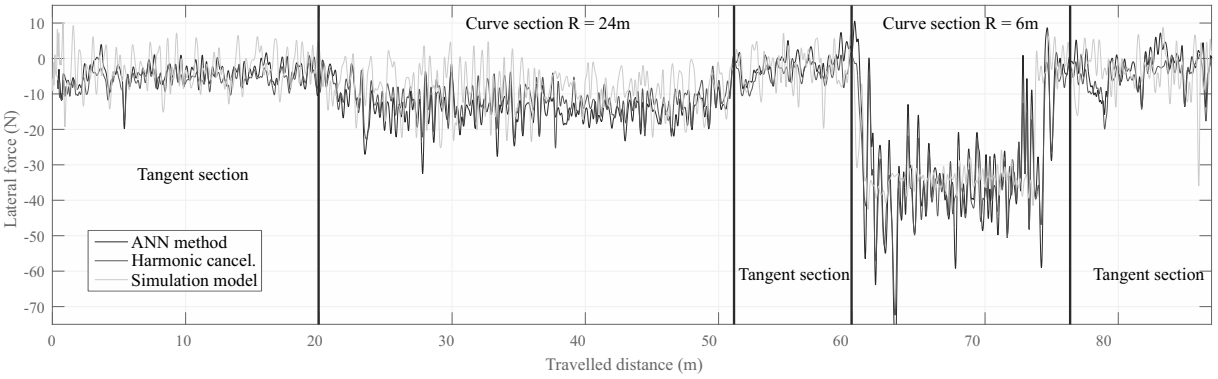


Figure 20: Applied lateral force on the instrumented wheel. Methods comparison in experiment 4

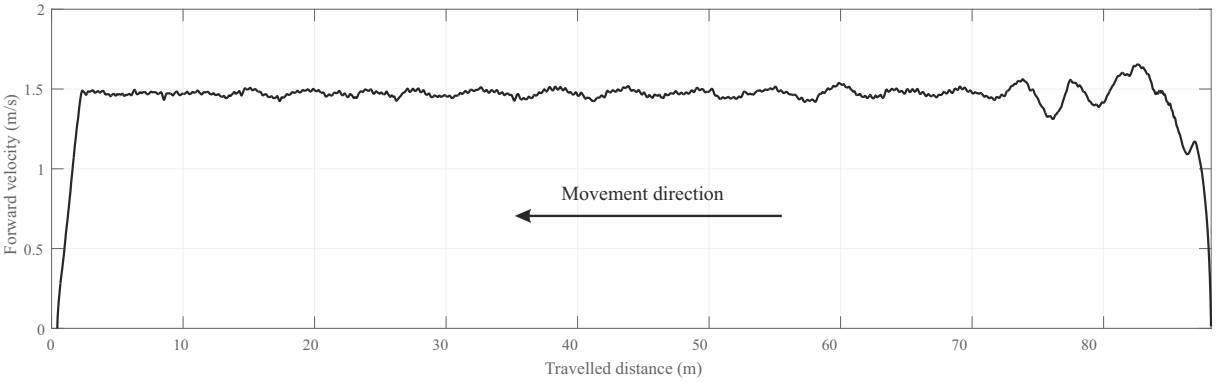


Figure 21: Vehicle's forward velocity

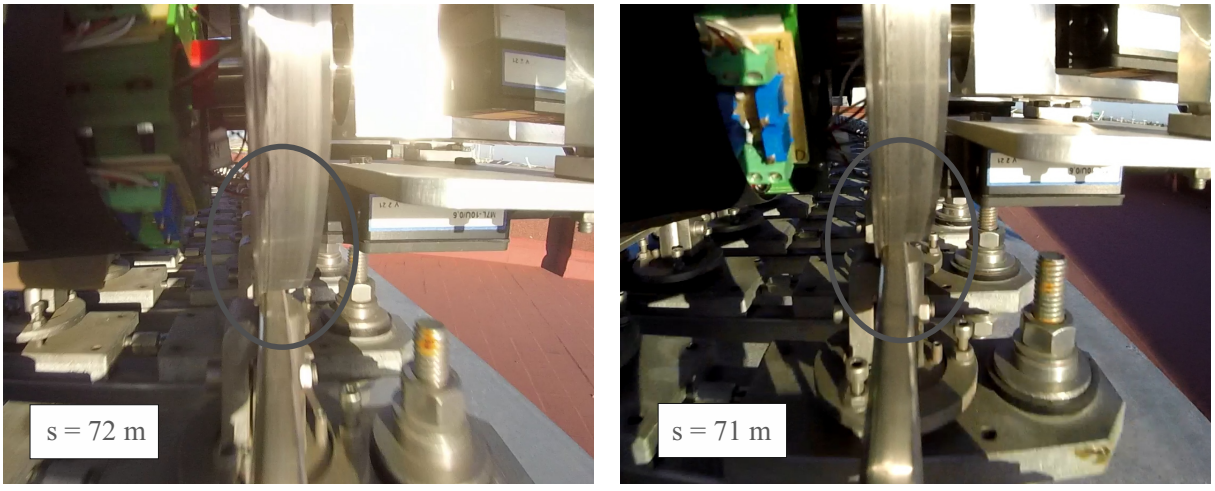


Figure 22: Instrumented wheel and rail interaction in the sharp radius curve at two different positions along the track

At this point, it must be clearly noted that, both the ANN and the harmonic cancellation method do not show a perfect agreement. Taking into account the excellent theoretical results obtained in Section

3, the reader could have expected a better accordance between both approaches when dealing with real experimental data, moreover when they use the same radial strains as inputs. The performance loss in relation to the theoretical experiments can be attributed to inaccuracies made during the calibration process of the dynamometric wheelset (imprecise FEM boundary conditions, inaccurate placement of sensor, etc.) but, this can not completely justify the differences between the ANN and harmonic cancellation approaches during their experimental comparison, precisely because such possible inaccuracies are common and identical to both measuring methods. It is the ANN training process which plays a fundamental role here. The ANN proposed in this work has been trained using synthetic data drawn from the FEM assuming different combinations of lateral and vertical forces and different forward velocities of the wheelset. Using this information, the network learns how to estimate the applied lateral force on the instrumented wheel based on the measured radial strains on the wheel web. When the instrumented vehicle is on the track, other phenomena such as the variation of the contact point on the wheel, high frequency vibration induced by track irregularities, manufacturing imperfections such as small clearances between the bearing and the bearing boxes, etc. are also registered by the strain sensors. In such a way, the input data used in the NN is contaminated if compared with the synthetic data used in the theoretical experiments. These unknown data require that the network made its best force estimation based on the knowledge acquired during its training. On this basis, it cannot expected the ANN and the harmonic cancellation method shown equivalent results even when using the same real data due to the fact, the internal algorithm of the ANN is not the same as the harmonic cancellation method. It can be said that, the NN is intelligent and it adapts its response depending on the circumstances always in order to find an optimal solution.

6. Summary and conclusions

In this paper, an ANN based algorithm has been presented for the experimental measurement of wheel-rail contact forces. The algorithm uses as inputs the radial strains measured in the wheel-web of an instrumented wheel. This algorithm is intended to be a real alternative to a harmonic cancellation method [32] also presented in this work. The performance of both approaches has been analysed in detail using synthetic data first. Several ANN architectures with different numbers of hidden layers and neurons have been tested in order to find the most suitable architecture for this particular application. The ANN has been trained using different training algorithms and synthesised data drawn from a FEM of the instrumented wheel. A $\{10-5\}$ network trained with the *Levenberg-Marquardt* algorithm proved to be a good solution for this particular application. Several tests have been carried out on a experimental 5-inch-wide scaled track in order to demonstrate the real potential of an ANN for the wheel-rail experimental contact force measurement. A 1:10 instrumented scaled bogie has been used in these experiments. The vehicle includes a dynamometric wheelset equipped with strain gauges for the measurement of the applied lateral force on the instrumented wheel. As a result, it has been observed that the ANN is able to estimate the applied lateral force with similar results to the classical harmonic cancellation method in a simpler computational manner and requiring a lesser number of sensors involved.

In view of the obtained results in this research, it can be concluded that an ANN is a valid solution

for the experimental measurement of wheel-rail lateral contact forces. As main scientific contribution, the ANN has proven to be a fast and reliable alternative, even using a reduced number of inputs, than the harmonic cancellation method. This latter approach mandatory requires an encoder sensor for the measurement of the instantaneous angular position of the wheel with respect to point of contact. However, the ANN is able to satisfactorily estimate the lateral force using exclusively strain measurements even considering a variable forward velocity of the vehicle. In such a way the ANN demonstrates being not dependent on the wheelset forward velocity. In this work, the experimental results obtained with the ANN and the classical method have also been compared with the simulated force drawn from a computational model of the vehicle. It is observed how both experimental approaches show a good accordance in magnitude and frequency content with the simulated data drawn from the multibody model. As conclusion, the use of ANNs can be considered as a reliable and accurate method to measure lateral contact forces with a reduced number of inputs and in an efficient computational manner. Since the dynamics of railway vehicles has been traditionally based on non-linear and computationally non-efficient multibody simulation models, the use of ANN might be a solution for an onboard evaluation of lateral contact forces with real-time capabilities. The method presented in this work can be extended to a full scaled vehicle. In that case, the ANN could also be used to measured the applied vertical load provided that a large number strain sensors can be installed in the wheel-web.

Having a reliable and computationally efficient artificial intelligence method for the analysis of the wheel-rail interaction represents a great step forward for the railways engineering. From this perspective, other problems of great interest for the railways industry such as the online measurement of contact points, vehicle's stability, irregularity identification, wheel and rail profiles wear, corrugation, etc., could be addressed in a more efficient way than using sophisticated and low efficient (although accurate and effective) traditional mechanical engineering methods.

Acknowledgements

This research was supported by the Spanish Ministry of Economy and Competitiveness under the project reference TRA2017-86355-C2-1-R. This support is gratefully acknowledged.

References

[1] S. O. Haykin, M. University, O. Canada, Neural Networks: A Comprehensive Foundation, Pearson, 1999.

[2] A. Y. Zomaya, Handbook of nature-inspired and innovative computing, Springer, 2006. doi:https://doi.org/10.1007/0-387-27705-6.

[3] P. P. Cruz, Inteligencia artificial con aplicaciones a la ingeniería, Alfaomega, 2010.

[4] A. P. Engelbrecht, Computational Intelligence: An Introduction, Wiley, 2007.

[5] S. Falomi, M. Malvezzi, E. Meli, A. Rindi, Determination of wheel–rail contact points: comparison between classical and neural network based procedures, Meccanica 44 (2009) 661–686. doi:10.1007/s11012-009-9202-6.

[6] J. L. Escalona, J. F. Aceituno, Multibody simulation of railway vehicles with contact lookup tables, International Journal of Mechanical Sciences 155 (2019) 571–582. doi:https://doi.org/10.1016/j.ijmecsci.2018.01.020.

[7] T. Gajdar, I. Rudas, Y. Suda, Neural network based estimation of friction coefficient of wheel and rail, in: IEEE International Conference on Intelligent Engineering Systems, Proceedings, INES, IEEE, 1997, pp. 315–318.

[8] M. Malvezzi, L. Pugi, S. Papini, A. Rindi, P. Toni, Identification of a wheel-rail adhesion coefficient from experimental data during braking tests, Proceedings of the Institution of Mechanical Engineers, Part F: Journal of Rail and Rapid Transit 227 (2) (2013) 128–139. doi:10.1177/0954409712458490.

[9] J. Sadeghi, H. Askarinejad, Application of neural networks in evaluation of railway track quality condition, Journal of Mechanical Science and Technology 26 (2012) 113–122. doi:10.1007/s12206-011-1016-5.

[10] J.-H. Chou, J. Ghaboussi, R. Clark, Application of Neural Networks to the Inspection of Railroad Rail, Springer US, Boston, MA, 1999, pp. 2121–2128. doi:10.1007/978-1-4615-4791-4_272.

[11] M. Chenariyan Nakhaee, D. Hiemstra, M. Stoelinga, M. van Noort, The recent applications of machine learning in rail track maintenance: A survey, in: S. Collart-Dutilleul, T. Lecomte, A. Romanovsky (Eds.), Reliability, Safety, and Security of Railway Systems. Modelling, Analysis, Verification, and Certification, Springer International Publishing, Cham, 2019, pp. 91–105.

[12] J. Chen, Z. Liu, H. Wang, A. Nuñez, Z. Han, Automatic defect detection of fasteners on the catenary support device using deep convolutional neural network, IEEE Transactions on Instrumentation and Measurement 67 (2) (2018) 257–269. doi:10.1109/TIM.2017.2775345.

[13] Y. Cheng, H. Zhao, Fault detection and diagnosis for railway switching points using fuzzy neural network, 2015 IEEE 10th Conference on Industrial Electronics and Applications (ICIEA) (2015) 860–865doi:10.1109/ICIEA.2015.7334231.

[14] J. Yin, W. Zhao, Fault diagnosis network design for vehicle on-board equipments of high-speed railway: A deep learning approach, Engineering Applications of Artificial Intelligence 56 (2016) 250 – 259. doi:https://doi.org/10.1016/j.engappai.2016.10.002.

[15] A. Shebani, S. Iwnicki, Prediction of wheel and rail wear under different contact conditions using artificial neural networks, Wear 406-407 (2018) 173 – 184. doi:https://doi.org/10.1016/j.wear.2018.01.007.

[16] H. Yuan, H. Chen, S. Liu, J. Lin, X. Luo, A deep convolutional neural network for detection of rail surface defect, 2019 IEEE Vehicle Power and Propulsion Conference (VPPC) (2019) 1–4doi:10.1109/VPPC46532.2019.8952236.

[17] S. Bruni, J. Meijaard, G. Rill, A. L. Schwab, State-of-the-art and challenges of railway and road vehicle dynamics with multibody dynamics approaches, Multibody System Dynamics 49 (2020) 1–32. doi:https://doi.org/10.1007/s11044-020-09735-z.

[18] F. Xia, C. Cole, P. Wolfs, Grey box-based inverse wagon model to predict wheel–rail contact forces from measured wagon body responses, Vehicle System Dynamics 46 (S1) (2008) 469–479. doi:10.1080/00423110801993102.

[19] F. Xia, C. Cole, P. Wolfs, An inverse railway wagon model and its applications, Vehicle system dynamics 45 (6) (2007) 583–605. doi:10.1080/00423110601079151.

[20] J. L. Escalona, J. F. Aceituno, P. Urda, O. Balling, Railroad multibody simulation with the knife-edge-equivalent wheel-rail constraint equations, Multibody System Dynamics 48 (2019) 373–402.

[21] J. F. Aceituno, P. Urda, E. Briales, J. L. Escalona, Analysis of the two-point wheel-rail contact scenario using the knife-edge-equivalent contact constraint method, Mechanism and Machine Theory 148 (2020) 103803. doi:https://doi.org/10.1016/j.mechmachtheory.2020.103803.

[22] S. Falomi, M. Malvezzi, E. Meli, Multibody modeling of railway vehicles: Innovative algorithms for the detection of wheel-rail contact points, Wear 271 (1) (2011) 453 – 461, proceedings of the 8th International Conference on Contact Mechanics and Wear of Rail / Wheel Systems, Florence, 2009. doi:https://doi.org/10.1016/j.wear.2010.10.039.

[23] Y. Li, J. Liu, K. Wang, J. Lin, C. Wang, Continuous measurement method of wheel/rail contact force based on neural network, 2011, pp. 2533–2537. doi:10.1061/41184(419)418.

[24] L. Gualano, S. Iwnicki, P. Ponnapalli, P. Allen, et al., Prediction of wheel-rail forces, derailment and passenger comfort using artificial neural networks. (01 2006).

[25] M. Yu, P. Yang, S. Wei, Railway obstacle detection algorithm using neural network, AIP Conference Proceedings (2018). doi:https://doi.org/10.1063/1.5039091.

[26] T. Ye, B. Wang, P. Song, J. Li, Automatic railway traffic object detection system using feature fusion refine neural network under shunting mode, Sensors 18 (2018). doi:https://doi.org/10.3390/s18061916.

[27] J. Hu, B. Noche, Application of artificial neuron network in analysis of railway delays, Open Journal of Social Sciences 4 (2016) 59–68. doi:10.4236/jss.2016.411005.

[28] M. Gallo, G. De Luca, L. DaAcierno, M. Botte, Artificial neural networks for forecasting passenger flows on metro lines, Sensors 19 (15) (2019). doi:10.3390/s19153424.

[29] S. Dundar, I. Sahin, Train re-scheduling with genetic algorithms and artificial neural networks for single-track railways, Transportation Research Part C: Emerging Technologies 27 (2013) 1 – 15, selected papers from the Seventh Triennial Symposium on Transportation Analysis (TRISTAN VII). doi:https://doi.org/10.1016/j.trc.2012.11.001.

[30] G. Paneiro, F. O. Durao, M. costa e Silva, P. F. Neves, Artificial neural network model for ground vibration amplitudes prediction due to light railway traffic in urban areas, Neural Computing and Applications 29 (2018) 1045–1057. doi:https://doi.org/10.1007/s00521-016-2625-9.

[31] Y. Changwei, L. Zonghao, G. Xueyan, Y. Wenying, J. Jing, , Z. Liang, Application of bp neural network model in risk evaluation of railway construction, Complexity (2019). doi:https://doi.org/10.1155/2019/2946158.

[32] M. D. Gutiérrez-López, J. G. de Jalón, A. Cubillo, A novel method for producing low cost dynamometric wheels based on harmonic elimination techniques, Mechanical Systems and Signal Processing 52 (2015) 577–599. doi:https://doi.org/10.1016/j.ymssp.2014.06.010.

[33] E. Gomez, J. Giménez, A. Alonso, Method for the reduction of measurement errors associated to the wheel rotation in railway dynamometric wheelsets, Mechanical Systems and Signal Processing 25 (8) (2011) 3062–3077. doi:https://doi.org/10.1016/j.ymssp.2011.05.006.

[34] S. Muñoz, J. F. Aceituno, P. Urda, J. L. Escalona, Multibody model of railway vehicles with weakly coupled vertical and lateral dynamics, Mechanical Systems and Signal Processing 115 (2019) 570–592. doi:https://doi.org/10.1016/j.ymssp.2018.06.019.

[35] E. García, J. A. Fernández, L. Baeza, F. J. Fuenmayor, Método de determinación de las fuerzas en el contacto rueda-carril en vehículos ferroviarios, Oficina Española de Patentes y Marcas ES 2 436 692 B1 (2014).

[36] P. Urda, S. Munoz, J. F. Aceituno, J. L. Escalona, Wheel-rail contact force measurement using strain gauges and distance lasers on a scaled railway vehicle, Mechanical Systems and Signal Processing 138 (2020) 106555. doi:https://doi.org/10.1016/j.ymssp.2019.106555.

[37] J. Pérez, J. A. Cabrera, J. J. Castillo, J. M. Velasco, Bio-inspired spiking neural network for nonlinear systems control, Neural Networks 104 (2018) 15 – 25. doi:https://doi.org/10.1016/j.neunet.2018.04.002.

[38] M. H. Beale, M. T. Hagan, H. B. Demuth, Neural Network Tollbox™ 7, MathWorks, 2010.

[39] K. Hornik, M. Stinchcombe, H. White, Multilayer feedforward networks are universal approximators, Neural Networks 2 (5) (1989) 359 – 366. doi:https://doi.org/10.1016/0893-6080(89)90020-8.

[40] J. F. Aceituno, R. Chamorro, D. García-Vallejo, J. L. Escalona, On the design of a scaled railroad vehicle for the validation of computational models, Mechanism and Machine Theory 115 (2017) 60–76. doi:https://doi.org/10.1016/j.mechmachtheory.2017.04.015.

[41] K. Hoffmann, An introduction to stress analysis and transducer design using strain gauges, HBM test and measurement (2012) 218–300.